

## ■ Peptide Nanofibers

# **Enhanced Stability of Peptide Nanofibers Coated with a Conformal Layer of Polydopamine**

Mingyang Ji and Jon R. Parquette\*[a]

Abstract: The susceptibility of self-assembled materials to changes of environmental conditions and mechanical forces often limits their utility for many applications. In this work, the surface of nanofibers formed by β-sheet peptide self-assemblies were coated by polydopamine (PDA) deposition. This conformal coating process rendered the nanofiber dimensions and internal  $\pi$ -stacking chirality impervious to changes in pH, temperature, and physical processing by spin-coating onto a silicon wafer. Whereas sonication-induced shearing of the dopamine/naphthalenediimide-dilysine (DA/NDI-KK) composite irreversibly shortened the nanofibers into 100-200 nm segments, the uncoated nanofibers unraveled into single strands upon similar treatment. Additionally, the PDA-coated nanofibers could be wrapped by an additional layer comprised of a positively charged polyelectrolyte polymer.

## Introduction

The self-assembly of peptides and their derivatives offers a reliable method to create a wide array of functional nanomaterials, especially for application to biomedical and optoelectronic problems.[1] Peptides can be readily tuned to assemble into a diverse range of nanostructures with structural and functional properties enhanced by the intermolecular interactions among the component monomers. For example, the properties of optoelectronic materials depend on the morphology, dimensions, and the nature of the inter-chromophore  $\pi$ – $\pi$  interactions, which are dictated by the assembly conditions.[2] However, these materials must be compatible with device processing conditions and exhibit long-term environmental stability.[3] Biomedical platforms face a similar challenge to remain stable at very low therapeutic concentrations in a rapidly fluctuating, extracellular environment containing salts, serum albumins, and the potential for enzymatic degradation. [4,5] However, self-assembled nanostructures rely on weak, noncovalent forces to maintain their structural integrity and often degrade when exposed to physical forces or environmental circumstances that depart from the conditions of their assembly. Strategies to stabilize the essential structural features of nanomaterials over a wide range of conditions will be necessary for them to find widespread applicability in these areas.

Self-assembled gels depend on inherently dynamic, noncovalent interactions to produce the polymeric network that gives rise to the physical properties of the gel.<sup>[6]</sup> Thus, efforts

[a] Dr. M. Ji, Prof. Dr. J. R. Parquette Department of Chemistry, The Ohio State University 100W. 18th Ave., Columbus, Ohio 43210 (USA) E-mail: parquette.1@osu.edu

Supporting information and the ORCID identification number(s) for the author(s) of this article can be found under:

Wiley Online Library

https://doi.org/10.1002/chem.202000403.

to enhance the physical/mechanical stability of peptide hydrogels have generally relied on a "covalent capture" strategy to render the fluxional polymer network permanent through chemical or enzymatic cross-linking.<sup>[8]</sup> The lateral cross-linking of reactive surface groups on discrete nanostructures can also be used to create a rigid outer shell that improves structural integrity. [8h] This process has been used to covalently capture self-assembled nanotubes, [8i] to create new polymeric structures from an original nanostructure used as a sacrificial template, [9] and to stabilize metallic nanoparticles against thermal degradation. [9b] However, the applicability of this strategy is limited by the need to design a new, suitably functionalized monomer that assembles in a similar manner as the original system lacking the cross-linking functionality. This process also leads to aggregation when the cross-linked structure exhibits lower solubility or when interparticle/fiber cross-links are formed.[8g,9b] These problems can often be ameliorated by crosslinking the nanostructures at low concentrations; however, the utility of this option is dictated by the critical aggregation concentration of the nanostructure.

We previously showed that ionic polymers could be used to coat the surface of self-assembled nanotubes.<sup>[10]</sup> This wrapping process could be used to prevent nanotubes, shortened by sonication, from re-assembling into their prior elongated states.[11] However, the polyelectrolyte coatings could be displaced by environmental factors, such as pH, ionic strength, and solvent, thereby limiting the generality of this method. [12] We reasoned that coating nanostructures with polydopamine (PDA) would produce robust composites more capable of sustaining changes of solvent, pH, or ionic strength. Polydopamine coatings on substrates are produced by the in situ, oxidative polymerization of dopamine (DA) in weak alkaline solutions.[13] This process deposits a conformal, highly cross-linked PDA film that adheres to substrates by forming covalent and noncovalent bonds.[14] The PDA layer exhibits inherent reactivi-

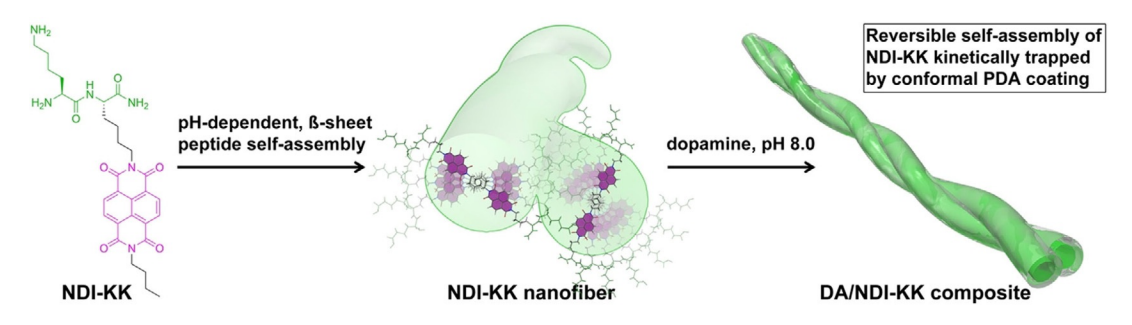
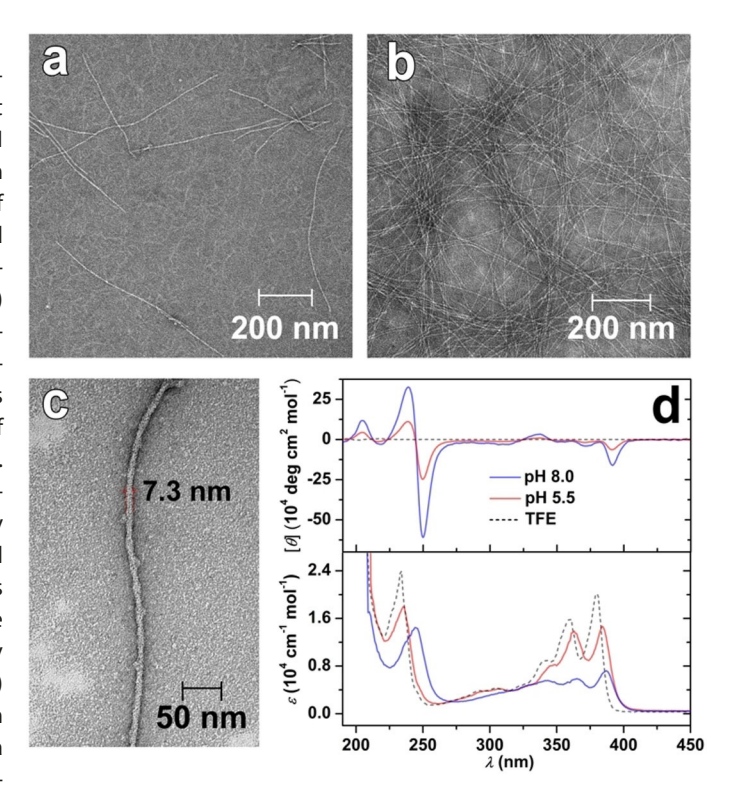


Figure 1. Graphical representation of the pH-dependent self-assembly of NDI-KK nanofibers stabilized by the formation of conformal PDA coating.

ty toward nucleophilic groups, such as amines and thiols, due to the presence of electrophilic catechol quinone components of the coating. This reactivity allows for covalent bonds to form during the coating process and offers the potential for post-polymerization surface functionalization. These features afford PDA a unique ability to conformally coat virtually any type of surface. In this work, we report that nanofibers formed by the self-assembly of a naphthalenediimide—dilysine peptide (NDI–KK) were stabilized against changes in pH, temperature, and physical processing by the deposition of a conformal layer of PDA onto the nanofibers surface (Figure 1). The surface of the DA/NDI–KK nanofibers were subsequently coated with a fluorescent, polyelectrolyte polymer.

**Results and Discussion** 

The structure of nanomaterials created by peptide self-assembly critically depends on extrinsic environmental factors that modulate the nature of interpeptide interactions. Thus, the pH responsivity of several peptide-based nanomaterials has been well-documented.<sup>[19]</sup> In order to demonstrate the capability of a PDA coating to stabilize the structure of a self-assembled nanostructure, we chose to study nanofibers, which were derived from the assembly of a dilysine-NDI peptide (NDI-KK) and were not stable at low pH values. Previously, we developed a series of dipeptide-NDI conjugates that underwent βsheet assembly into 1D nanostructures in water.<sup>[20]</sup> In this series of peptides, intermolecular electrostatic repulsions of protonated lysine side chains attenuated the assembly process. Thus, in contrast to peptides with a single-charged lysine residue, the self-assembly of NDI-KK was severely hampered by the additional positive charge contributed by the N-terminal ammonium group, resulting in no observable nanostructures at concentrations below 25 mm. To lower the charge of the peptide, we explored the pH dependence of the self-assembly of NDI-KK. Samples of NDI-KK were prepared in water (10 mm) then adjusted to either pH 5.5 or 8.0. After 12 h, transmission electron microscopy (TEM) imaging revealed the presence of a few, short nanofiber segments at pH 5.5 that evolved into micrometer-long nanofibers with uniform diameters of (7  $\pm$  1) nm at pH 8.0 (Figures 2a-c). Atomic force microscopy (AFM) images of NDI-KK at pH 8.0 (Figure 3a) indicated helically twisted nanofibrils with a pitch length of  $(60\pm3)$  nm and cross-sectional heights of approximately 7 nm. At both pH values and in trifluoroethanol (TFE), NDI–KK exhibited UV/Vis absorptions at 244 (pH 8.0), 236 (pH 5.5), or 234 (TFE) (band II) and 300–400 nm (band I), which corresponded to  $\pi$ – $\pi^*$  transitions polarized along the short and long axis of the NDI chromophore, respectively. The decreasing intensity of the band I absorptions going from TFE to pH 5.5 and pH 8.0 in water were consistent with the progressive onset of self-assembly at higher pH values. Similarly, the most red-shifted band at pH 8.0 was indicative of J-type  $\pi$ – $\pi$  stacking of NDI chromophores in water. Specifically, as the pH increased from 5.5 to 8.0, the redshifts, compared with that of TFE, increased from 4 to 7 nm for band I and from 2 to 10 nm for band II, respectively. The circular dichroic (CD) spectra of NDI–KK (Figure 2d) ex-



**Figure 2.** TEM images of the pH-dependent self-assembly of NDI–KK in water at a) pH 5.5 and b,c) 8.0. All NDI–KK samples were prepared at a concentration of 10 mm and adjusted to the desired pH with 1 m NaOH/HCI. After a 12 h incubation, the samples were diluted to 1 mm for TEM imaging. d) CD and UV/Vis spectra of NDI–KK in water (250  $\mu$ m, freshly diluted from 10 mm after incubation) at pH 5.5 and 8.0, and in TFE (100  $\mu$ m).

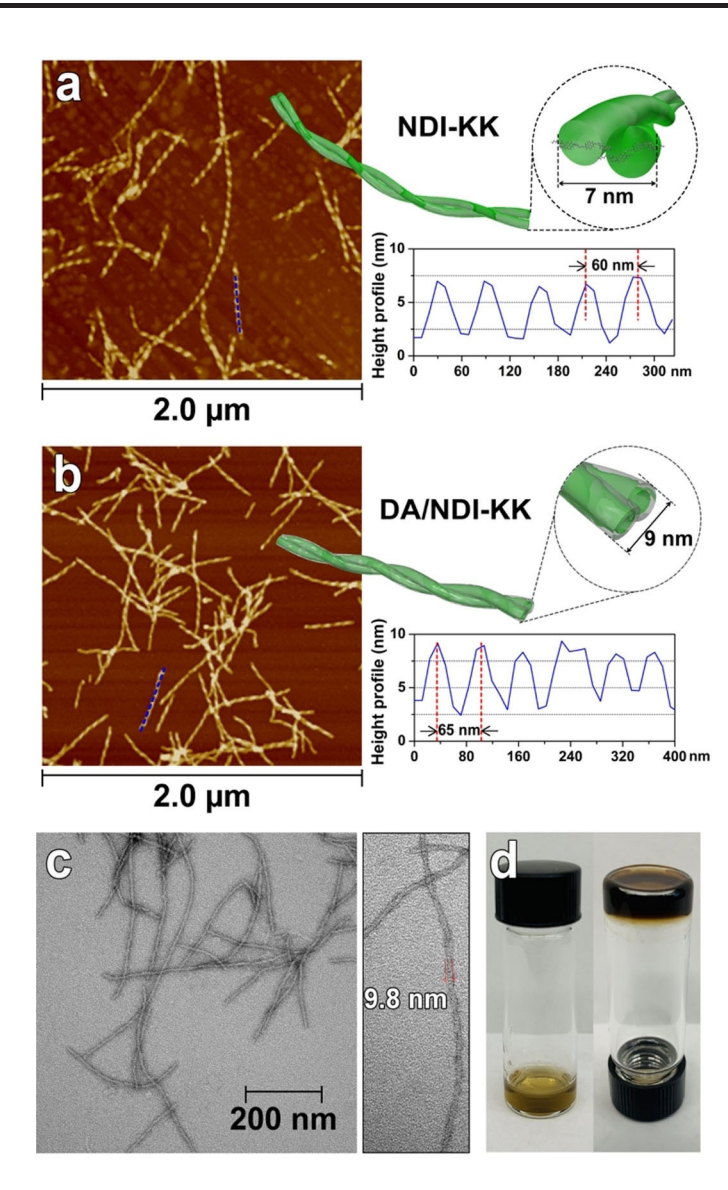


**Figure 3.** AFM images and height profiles of a) NDI–KK and b) DA/NDI–KK (1:1, n/n) nanofibers in water (pH 8.0). NDI–KK and DA/NDI–KK were prepared in water (10 mm with respect to NDI–KK) at pH 8.0 and freshly diluted to 1 mm for AFM imaging. c) TEM images of DA/NDI–KK (1:1, n/n) after ultracentrifuge at 80 000 rpm (312  $000 \times g$ ) for 30 min. d) Picture of DA/NDI–KK (1:1, n/n) upon dissolving at pH 8.0 and the resulting DA/NDI–KK hydrogel (1.0 wt%) after incubation at 25 °C for 24 h.

hibited significantly more intense transitions corresponding to both absorption bands at pH 8.0 than at pH 5.5; or in TFE, in which a flat CD signal was displayed, indicative of a monomeric state. The negative, bisignet excitonic couplet, centered at around 242 nm of NDI–KK in water at both pH values, reflects a left-handed, *M*-type helical arrangement of adjacent NDI chromophores within the nanofiber. These observations confirm that the self-assembly of NDI–KK could be initiated by increasing the pH to reduce the electrostatic repulsions that attenuate assembly at lower pH values.

At pH 8.0, assembled NDI–KK nanofibers exhibited considerable stability to dilution. Samples of NDI–KK were prepared by incubating at 10 mm for 12 h, then diluting to 1 and 0.1 mm. After 12 h at  $25\,^{\circ}$ C, the UV/Vis and CD spectra were un-

www.chemeurj.org

changed, indicating a stable assembled state at 0.1 mm at pH 8.0 (Figures S1 and S2 in the Supporting Information). The role of charge repulsion, as dictated by pH, in modulating the self-assembly process was further explored by measuring ζ-potentials. Accordingly, the assembled NDI-KK nanofibers (10 mm, pH 8.0) were diluted to 1 mm, and the ζ-potential was recorded over a pH range from 3–9 (Figure S3 a). The  $\zeta$ -potentials of the samples decreased from (48.8  $\pm$  9.35) to (33.8  $\pm$ 3.91) mV, as the pH rose from 7.4 to 9.0. In contrast, at pH values below 6.5, short nanofibers were mixed with small aggregates and monomers, which resulted in unreliable  $\xi$ -potential measurements (Figure S3 a). Nanofiber dissociation at pH 3.0 was confirmed by TEM imaging, which only revealed a few short fibrils (Figure S4). Similarly, the red-shifted absorption bands that were present at pH 8.0 were blue shifted at pH 3.0, and the corresponding CD spectrum was flat, indicating that NDI-KK resided in a predominantly monomeric state (Figures 4a and S5).

The high pH sensitivity of the NDI–KK nanofibers provided an opportunity to investigate the potential for a conformal PDA coating to stabilize the fibers under adverse conditions, such as low pH, that normally induce disassembly. The basic environment required to induce the self-assembly of NDI–KK also promoted the oxidative self-polymerization of dopamine. [13,23] Therefore, to deposit a conformal coating of PDA on the surface of the nanofibers, an aqueous solution of pre-assembled NDI–KK nanofibers (10 mm, pH 8.0, 12 h) was treated

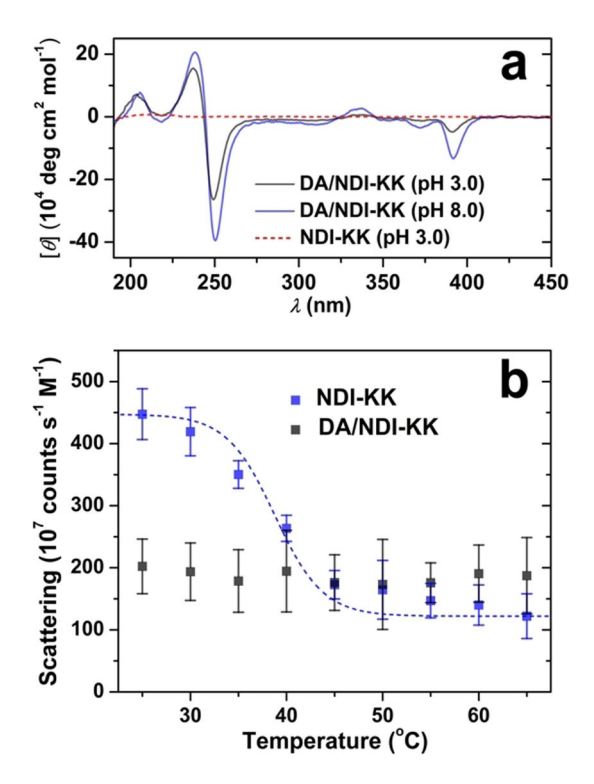


Figure 4. a) CD spectra of DA/NDI–KK (1:1, n/n) at pH 3.0 and 8.0 in water. The pH 3.0 sample was adjusted from pH 8.0 and equilibrated at pH 3.0 for 24 h before spectral collection. As a comparison, NDI–KK at pH 3.0 showed no CD signature (dashed red line). b) Molar scattering intensity of NDI–KK (0.1 mm, pH 7.0) and DA/NDI–KK (1:1, pH 7.0, 0.1 mm with respect to NDI–KK) upon heating. The dashed blue curve is given for eye guidance.



with dopamine hydrochloride (DA) to achieve a 1:1 (DA/NDI-KK) ratio. These conditions allowed the DA to polymerize onto the surface of the nanofibers. Thus, incubating this solution at pH 8.0 for 24 h at 25 °C induced the initially transparent mixture to transform into a dark-brown, self-supporting hydrogel composite (DA/NDI-KK, 1:1, n/n) (Figure 3 d). Polydopamine composites often form hydrogels because the adhesiveness of the dopamine-quinone surface structure promotes the formation of intermolecular junction points between the nanofibers.[24] The hydrogel was diluted with water and ultracentrifuged at 80 000 rpm (312 000  $\times$  g) for 30 min to isolate the DA/ NDI-KK composite within the pellet, separated from free NDI-KK monomer and dopamine/PDA oligomers, which remained in the supernatant under these conditions. The final molar ratio (DA/NDI-KK) was calculated to be 0.85:1 in the resulting composite pellet (Figure S6) after accounting for the dopamine and PDA found in the supernatant.

To optimize the coating thickness, the surface saturation point was determined by varying the feeding ratio of DA and NDI–KK (2:1, 1:1, and 1:2 (DA/NDI–KK)). After incubation at pH 8.0 for 12 h and pelleting by ultracentrifugation, the pellets and supernatants were collected. The UV absorption at 280 nm indicated that excess PDA and DA were present in the supernatants of the 2:1 sample, but not in the 1:1 and 2:1 samples. Furthermore, the TEM image of the 2:1 (DA/NDI–KK) composite showed that that DA/NDI–KK nanofibers were contaminated with large amounts of PDA nanoparticles (Figure S8). These experiments indicated that a 1:1 ratio represented the optimal feeding ratio.

To characterize the chemical composition of the nanofibers, we compared the C1s and N1s X-ray photoelectron spectra (XPS) of the parent NDI-KK and the composite DA/NDI-KK nanofibers (Figure S7). Although the resolution of XPS was not capable of differentiating segregated from composite PDA and NDI-KK nanostructures, UV/Vis analysis of the pellet obtained by ultracentrifugation indicated that the sample was not contaminated by PDA nanoparticles. The C1s spectrum of NDI-KK exhibited a peak at 288.3 eV, corresponding to amide groups (N-C=O) present in the peptide; whereas the spectra of DA/ NDI-KK composite showed additional peaks characteristic of the PDA layer (C=O (287.9 eV) and C-N/C-OH (286.2 eV))<sup>[25]</sup> The N1s spectrum of NDI-KK could be deconvoluted into two peaks at 400.1 and 399.2 eV, corresponding to (C=O)-N-(C= O)/N-(C=O)- and C-NH<sub>2</sub>, respectively. In contrast to the spectrum of NDI-KK, which was dominated by the amide/imide peak; the DA/NDI-KK spectrum had a larger C-NH2 component, consistent with the formation of a PDA coating on the NDI-KK surface.

Imaging by AFM and TEM showed the DA/NDI–KK composite as helical nanofibers that closely resembled the parent NDI–KK fibrils formed at pH 8.0, but with larger AFM cross-sectional heights [(9 $\pm$ 1) nm] and helical pitch values [(65 $\pm$ 4) nm] (Figures 3 b–c). Polydopamine films display a negative surface charge at pH 8.0.  $^{[26]}$  Therefore, the  $\zeta$ -potential of the starting NDI–KK fibers decreased from (47.5 $\pm$ 6.7) to (–5.6 $\pm$ 2.8) mV for the DA/NDI–KK composite. Remarkably, the CD spectrum of the composite remained nearly identical to the NDI–KK nano-

fibers, indicating that the long-range spatial organization and packing chirality of NDI chromophores was preserved in the DA/NDI-KK composite (Figures 4a and S9).

The DA/NDI-KK composites exhibited high stability to a drop in pH from 8.0 to 3.0. A freshly prepared and pelleted DA/NDI-KK (1:1, n/n) composite at pH 8.0 was adjusted to pH 3.0 and incubated at 25 °C. After 24 h, although a slight, 3 nm blueshift of the NDI band I absorption was observed (Figure S10 b), the intensity of the band was consistent with an assembled structure. Furthermore, the characteristic CD signature of the NDI-KK nanofibers, indicating an M-type helical packing of NDI chromophores, was largely intact under these conditions (Figures 4a and S10a). In comparison, the CD spectrum of the NDI-KK nanofibers (0.2 mm, pH 8.0) became flat within 10 min of acidification to pH 2.8 (Figure S19). Thus, the PDA coating protected the long-range, intermolecular organization within the nanofibers against the electrostatic repulsions induced at low pH. TEM images of the DA/NDI-KK (1:1, n/n) composite after equilibration at pH 3.0 (Figure S11) further confirmed that the composite nanofibers were preserved after acid treatment. It is noteworthy that, in contrast to the 2:1 and 1:1 DA/NDI-KK composites, 1:2 DA/NDI-KK did not effectively protect the nanofibers from dissociation at pH 3.0, resulting in a decreased CD signal (Figure S12) and the presence of very short nanofiber segments observable in corresponding TEM image (Figure S11 c).

We next explored the resilience of the composite to elevated temperatures. Due to the reversible nature of the self-assembled structure, heating the parent NDI-KK nanofibers (0.1 mm, pH 8.0) from 25 to 70 °C resulted in a progressive blueshift, due to dissociation of the nanofibers (Figure S1c). Based on this observation, the molar light scattering rates of DA/NDI-KK and the parent NDI-KK nanofibers, as measured by dynamic light scattering (DLS) were used to further evaluate changes in particle size distribution of the nanofibers at elevated temperatures (Figures 4b and S13).<sup>[27]</sup> At pH 7.0, the NDI-KK nanofibers (0.1 mm) exhibited a progressive decrease in the molar scattering intensity from 450 to  $120 \times 10^7$  counts s<sup>-1</sup> M<sup>-1</sup>, as the temperature rose from 25 to 65 °C. In contrast, the composite (pH 7.0, 0.1 mm with respect to NDI-KK) maintained very stable molar scattering intensities of approximately 200×  $10^7$  counts s<sup>-1</sup> m<sup>-1</sup> from 25–65 °C (Figure S13 a), indicative of higher temperature stability.<sup>[28]</sup> We further explored the stability of DA/NDI-KK at an unfavorable pH of 3.0, which dissociated pristine NDI-KK nanofibers lacking the conformal PDA coating. Even under these more rigorous conditions (pH 3.0, 0.1 mm), the composite retained molar scattering intensities of about  $250 \times 10^7$  counts s<sup>-1</sup> m<sup>-1</sup> from 25-65 °C (Figure S13 b).

We have previously observed that coaxial polymer–nano-tube composites could be created by electrostatically binding fluorescent polyelectrolytes to the surface of self-assembled NDI nanotubes. The polymer emission in these composites was efficiently quenched through electron/energy transfer between the polymer and the NDI nanotubes. The PDA coating on the NDI–KK nanofibers maintains a surface  $\zeta$ -potential that could be modulated by pH. In contrast to the uncoated NDI–KK nanofibers, which dissociated at lower pH values, the struc-

ture of the DA/NDI-KK composite was stable over a wide pH range. Thus, the  $\zeta$ -potential of the DA/NDI-KK composite could be adjusted from (39.8  $\pm$  3.4) to ( $-9.5 \pm$  3.2) mV over a pH range of 3.9-9.5 (Figure S3b). To investigate the ability of the DA/NDI-KK nanofibers to bind fluorescent polymers on the surface, a positively charged polyelectrolyte, poly(9,9-bis-[6'-(*N*,*N*,*N*,-trimethylammonium)hexyl]fluorene-co-alt-1,4-phenylene)bromide (PFQ-Br, 50 µм with respect to monomer), was titrated with DA/NDI-KK (1 mm with respect to NDI-KK) at pH 9.5 and 3.0, respectively (Figures 5 and S14). The emission of PFQ-Br was progressively decreased at both pH values as the DA/NDI-KK concentration increased from 0 to 36  $\mu M$ . The fluorescence decreased much more rapidly at pH 9.5 than at pH 3.0, as expected based on the pH dependence of the  $\zeta$ -potential of DA/NDI-KK. At pH 3.0, the positive ζ-potential of DA/ NDI-KK resulted in a repulsive electrostatic interaction between the polymer and DA/NDI-KK. Whereas, at pH 9.5, an attractive interaction between the negative  $\zeta$ -potential of DA/ NDI-KK and the polymer mediated a stronger binding interaction, leading to more efficient quenching of the polymer fluorescence. AFM imaging of the PFQ-Br/DA/NDI-KK nanofibers at

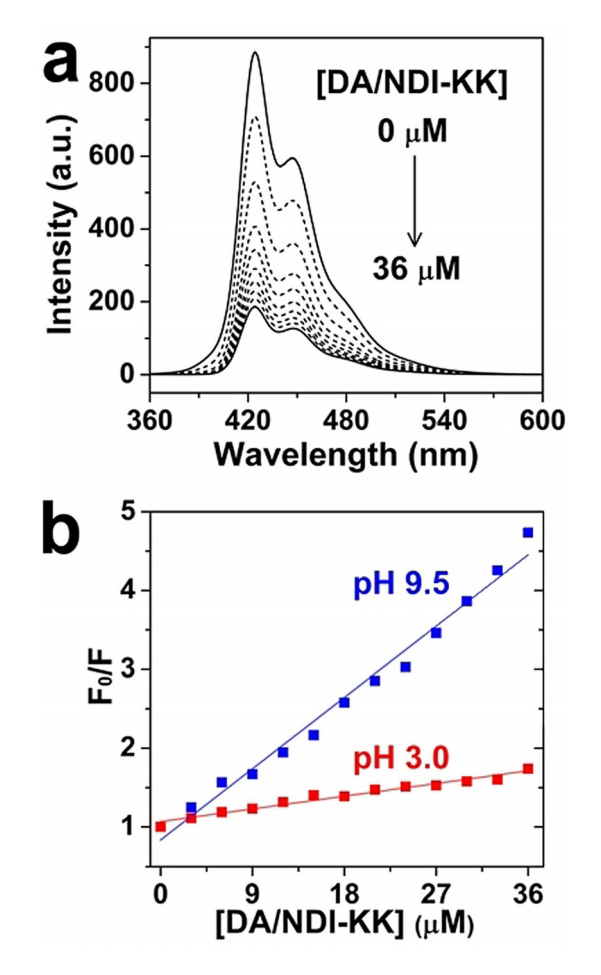


**Figure 5.** a) Fluorescence titration spectra of PFQ-Br (50 μm) upon addition of DA/NDI–KK at pH 9.5 in water. The arrow indicates the increase of quencher concentration (with respect to NDI–KK) from 0 to 36 μm. b) Emission intensity ratio ( $F_0/F$ ) at 424 nm as a function of [DA/NDI–KK] at pH 9.5 and 3.0 and the corresponding linear fitting curves.  $\lambda_{\rm Ex}$  = 330 nm.

pH 9.5 revealed larger height profiles than at pH 3.0 (Figure S15), due to greater coating of the composite nanofibers by PFQ-Br under basic conditions. In contrast to cationic PFQ-Br, the binding of anionic poly(*p*-phenylene ethynylene) (PPE-SO<sub>3</sub>Na), was strongest at pH values below 8.0. As shown in Figure S18, the emission of PPE-SO<sub>3</sub>Na was maximal above pH 11.0 and almost completely quenched below pH 8.0. These binding studies highlight the potential to modulate the DA/NDI-KK surface charge by pH to bind negatively and positively charged polymers.

Physical stability over a wide range of processing conditions and the ability to control fiber dimensions is critical for many applications of self-assembled nanomaterials. [29] We have previously reported that sonication-induced shear could be used to fragment NDI nanotubes into shorter segments.[11] However, the segments re-elongated after several hours due to the dynamic nature of self-assembly. Correspondingly, sonication of the NDI-KK fibers at pH 8.0 for 3 min at 20% amplitude (125 W, 20 kHz) (Figure S16) resulted in unwinding and fragmenting of the helically twisted fibers into single strands with shortened lengths of 100-200 nm, which also recovered the prior self-assembled states over 48 h. It is noteworthy that although sonication of the DA/NDI-KK composite fibers, under the same conditions, similarly fragmented into 100-200 nm segments, the helical nanofibers did not unwind and their dimensions remained unchanged after 48 h. The DA/NDI-KK composite also exhibited better mechanical stability and adhesion to the surface of silicon wafers. Thin layers prepared by spin coating a 1 mm solution of DA/NDI-KK at 2000 rpm for 60 s on silicon wafers produced a smooth and densely covered surface (Figure 6b) with a root mean square (RMS) roughness (Rq) of 3.48 nm (Figure S17e), which was comparable to a drop-casted DA/NDI-KK layer (Rq of 3.34 nm) (Figure S17 d), indicating excellent processing compatibility of DA/NDI-KK composite. In contrast, the shear forces of spin-coating pristine NDI-KK (1 mm) nanofibers resulted in poor coverage (Rq = 1.71 and 1.25 nm at 1000 and 2000 rpm, respectively) and fragmentation of the fibers (Figure 6a), compared with drop-casted NDI-KK (Rq = 3.22 nm) (Figure S17 a-c).

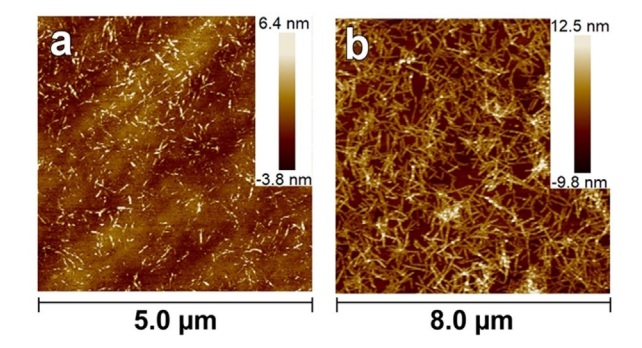


**Figure 6.** AFM images of a) pristine NDI–KK (1 mm) and b) DA/NDI–KK (ca. 1 mm with respect to NDI–KK) spin-coated on silicon wafers at 2000 rpm for 60 s.



## **Conclusions**

The structure of self-assembled nanomaterials must be stable under adverse conditions in order to find broad utility in opto-electronic applications. We have shown that deposition of a thin, conformal layer of PDA onto the surface of self-assembled NDI–KK peptide nanofibers renders them impervious to changes in pH, elevated temperature, concentration, and physical processing. In contrast to the pristine nanofibers, these extrinsic changes had no impact on the structural integrity of the PDA-coated nanofibers. Furthermore, the PDA surface could be wrapped with conjugated polymers to create polymer–nanofiber composites. We expect this strategy to enhance the range of applications that can be addressed by self-assembled materials.

## **Experimental Section**

## General methods

Atomic force microscopy (AFM) was conducted in tapping mode under a nitrogen atmosphere. Transmission electron microscopy (TEM) was carried out with Technai G2 Spirit instrument operating at 80 kV. <sup>1</sup>H and <sup>13</sup>C NMR were recorded at 400 MHz on a Bruker Avance III instrument. ESI mass spectra were recorded on a Bruker MicroTOF coupled with HPLC. All UV/Vis spectra were recorded with a SHIMADZU UV-2450 at 25 °C. All fluorescence spectroscopy was performed in a SHIMADZU RF-5301 using a cuvette with 3 mm pass length at 25 °C. Circular dichroism (CD) spectra were recorded using an AVIV 202 CD spectrometer at 25 °C. X-ray photoelectron spectroscopy (XPS) spectra were recorded using a Kratos Axis Ultra XPS spectrometer equipped with both monochromatic (AI) and dual (Mg and AI) X-ray sources. All reactions were performed under a nitrogen atmosphere.

## Preparation of DA/NDI-KK composites

NDI-KK was synthesized according to our previous work. [20] Freezedried NDI-KK (5.8 mg) was dissolved in 1.0 mL of HPLC-grade water to prepare homogeneous NDI-KK (10 mm) solution. With 1 m NaOH/HCl, the resulting NDI-KK solution was adjusted to desirable pH conditions as 3.0, 5.5, and 8.0 to complete the self-assembly within 12 h yielding transparent NDI-KK solutions. To 1.0 mL of NDI-KK nanofibers formed at pH 8.0, 1.9 mg of monomeric dopamine hydrochloride was added under vortexing to prepare DA/ NDI-KK (1:1, n/n) composite. After adjusting its pH to 8.0 again, the DA/NDI-KK (1:1, n/n) composite was incubated at 25°C for 24 h to form dark brown, self-supporting hydrogel. The hydrogel was diluted with water (9 mL) and centrifuged at 80,000 rpm  $(312,000 \times g)$  for 30 min, and the resulting pellets of DA/NDI-KK composite were collected for the following study. Due to the kinetic equilibrium of NDI–KK self-assembly,  $\approx$  12 mol % of NDI–KK and pprox 25 mol% of dopamine/PDA oligomers were left in the supernatant, resulting in a final molar ratio (DA/NDI-KK) of 0.85:1 in the composite pellet.

## Dynamic light scattering (DLS)

The scattering rate of the samples was determined by DLS measurement on a Malvern Zetasizer NanoZS system with folded capillary zeta cells (DTS1070) and obtained scattering count rates were normalized by the concentration of the solution to yield the molar

scattering rate. The folded capillary cell loaded with freshly prepared sample was inserted into the equipment chamber with preset temperatures to equilibrate for 10 min before each measurement. After equilibration, samples were taken 3–5 measurements at each temperature and each measurement was averaged from automatically determined 10–15 runs with a run duration of 10 s.

#### Transmission electron microscopy (TEM)

Re-dispersed pellets of DA/NDI-KK after ultracentrifugation (80,000 rpm, 30 min) were dropped on carbon-coated copper grids (Ted Pella, Inc.) for 10 min. After removal of excess solution, the sample grid was negatively stained with 2% (w/w) uranyl acetate solution. The dried specimen was observed with Technai G2 Spirit TEM instrument operating at 80 keV.

#### Atomic force microscopy (AFM)

AFM images were collected on Bruker AXS Dimension Icon Atomic Force Microscope under a nitrogen atmosphere in tapping mode using silicon tips (SCANASYST-AIR, Bruker). Re-dispersed pellets of DA/NDI–KK were dropped on freshly cleaved mica and allowed to dry for 30 min before imaging. AFM images  $(3.0\times3.0~\mu\text{m})$  were taken at a line frequency of 0.5 Hz and at a resolution of  $512\times512$  pixels. Obtained AFM images were analyzed with Bruker Nano-Scope Analysis (version 1.40) software.

#### Circular dichroism (CD) spectroscopy

CD spectra were recorded on an AVIV 202 CD spectrometer equipped with a Peltier temperature controller under a nitrogen atmosphere. Spectra were collected at 25 °C in a quartz cell with 1 mm path length over a wavelength range of 190–650 nm with a step size of 0.5 nm. All scans were conducted at continuous mode at the scanning speed of 100 nm min<sup>-1</sup>. Each CD spectrum was averaged from 3 scans with a data integration time of 2 s.

#### X-ray photoelectron spectroscopy (XPS)

XPS spectra were recorded using a Kratos Axis Ultra XPS spectrometer using an Al K $\alpha$  X-ray source (1486.69 eV). The high-resolution spectra for individual elements were recorded by accumulating 8–16 sweeps at a 30 eV pass energy and 0.1 eV/step. All samples were cast on monocrystalline silicon wafer to perform the XPS measurements. All the spectra were calibrated with reference to the C–C binding energy at 285.0 eV. Data analysis and curve fitting were performed using Casa XPS software with a Gaussian–Lorentzian product function and nonlinear Shirley background subtraction.

## **Acknowledgements**

This work was supported by the National Science Foundation (CHE-1708390). We gratefully acknowledge the Center for Applied Plant Sciences (CAPS) at The Ohio State University for partial funding of this work. We also thank the Campus Microscopy & Imaging Facility at OSU for technical assistance and usage of the facility.



## **Conflict of interest**

The authors declare no conflict of interest.

**Keywords:** amyloid peptides · nanostructures optoelectronics · polydopamine · self-assembly · stability

- [1] M. J. Webber, E. A. Appel, E. W. Meijer, R. Langer, *Nat. Mater.* **2016**, *15*, 13–26.
- [2] J. D. Tovar, Acc. Chem. Res. 2013, 46, 1527 1537.
- [3] M. Kettner, Z. Mi, D. Kälblein, J. Brill, P. W. M. Blom, R. T. Weitz, Adv. Electron. Mater. 2019, 5, 1900295.
- [4] J. Li, R. Xing, S. Bai, X. Yan, Soft Matter 2019, 15, 1704-1715.
- [5] H. Hosseinkhani, P. D. Hong, D. S. Yu, Chem. Rev. 2013, 113, 4837 4861.
- [6] a) A. Dasgupta, J. H. Mondal, D. Das, RSC Adv. 2013, 3, 9117-9149;
  b) B. O. Okesola, D. K. Smith, Chem. Soc. Rev. 2016, 45, 4226-4251.
- [7] L. J. Prins, P. Scrimin, Angew. Chem. Int. Ed. 2009, 48, 2288–2306; Angew. Chem. 2009, 121, 2324–2343.
- [8] a) T. Chen, K. Hou, Q. Ren, G. Chen, P. Wei, M. Zhu, Macromol. Rapid Commun. 2018, 39, 1800337; b) J. D. Hartgerink, E. Beniash, S. I. Stupp, Science 2001, 294, 1684-1688; c) L. Aulisa, H. Dong, J. D. Hartgerink, Biomacromolecules 2009, 10, 2694-2698; d) L. Chronopoulou, M. Daniele, V. Perez, A. Gentili, T. Gasperi, S. Lupi, C. Palocci, Process Biochem. 2018, 70, 110-116; e) W. Liyanage, H. A. Ardona, H. Q. Mao, J. D. Tovar, Bioconjugate Chem. 2017, 28, 751-759; f) M. D. Konieczynska, M. W. Grinstaff, Acc. Chem. Res. 2017, 50, 151-160; g) S. H. Kim, Y. Sun, J. A. Kaplan, M. W. Grinstaff, J. R. Parquette, New J. Chem. 2015, 39, 3225 -3228; h) X. Liu, A. Basu, J. Organomet. Chem. 2006, 691, 5148-5154; i) W. Jin, T. Fukushima, A. Kosaka, M. Niki, N. Ishii, T. Aida, J. Am. Chem. Soc. 2005, 127, 8284-8285; j) J. R. Moffat, I. A. Coates, F. J. Leng, D. K. Smith, Langmuir 2009, 25, 8786-8793; k) D. Wu, W. Wang, D. Diaz-Dussan, Y.-Y. Peng, Y. Chen, R. Narain, D. G. Hall, Chem. Mater. 2019, 31, 4092-4102; I) B. D. Polizzotti, B. D. Fairbanks, K. S. Anseth, Biomacromolecules 2008, 9, 1084-1087.
- [9] a) Y. Liu, J. Goebl, Y. Yin, Chem. Soc. Rev. 2013, 42, 2610–2653; b) S. Koenig, V. Chechik, Langmuir 2006, 22, 5168–5173.
- [10] M. Ji, M. B. Dawadi, A. R. LaSalla, Y. Sun, D. A. Modarelli, J. R. Parquette, Langmuir 2017, 33, 9129–9136.
- [11] M. Ji, B. Daniels, A. Shieh, D. A. Modarelli, J. R. Parquette, Chem. Commun. 2017, 53, 12806–12809.
- [12] M. Ji, M. L. Mason, D. A. Modarelli, J. R. Parquette, Chem. Sci. 2019, 10, 7868 – 7877.
- [13] Y. Liu, K. Ai, L. Lu, Chem. Rev. 2014, 114, 5057 5115.

- [14] J. H. Ryu, P. B. Messersmith, H. Lee, ACS Appl. Mater. Interfaces 2018, 10, 7523 – 7540.
- [15] J. Liebscher, R. Mrowczynski, H. A. Scheidt, C. Filip, N. D. Hadade, R. Turcu, A. Bende, S. Beck, *Langmuir* 2013, 29, 10539 10548.
- [16] J. B. Wood, M. W. Szyndler, A. R. Halpern, K. Cho, R. M. Corn, *Langmuir* 2013, 29, 10868 10873.
- [17] C. Y. Chien, W. B. Tsai, ACS Appl. Mater. Interfaces 2013, 5, 6975-6983.
- [18] a) W. Ding, S. A. Chechetka, M. Masuda, T. Shimizu, M. Aoyagi, H. Minamikawa, E. Miyako, *Chem. Eur. J.* 2016, 22, 4345–4350; b) A. K. Awasthi, S. D. Bhagat, R. Ramakrishnan, A. Srivastava, *Chem. Eur. J.* 2019, 25, 12905–12910.
- [19] a) S. Tsonchev, K. L. Niece, G. C. Schatz, M. A. Ratner, S. I. Stupp, J. Phys. Chem. B 2008, 112, 441–447; b) M. Hatip Koc, G. Cinar Ciftci, S. Baday, V. Castelletto, I. W. Hamley, M. O. Guler, Langmuir 2017, 33, 7947–7956; c) Y. R. Chen, H. X. Gan, Y. W. Tong, Macromolecules 2015, 48, 2647–2653; d) M. L. Mason, R. F. Lalisse, T. J. Finnegan, C. M. Hadad, D. A. Modarelli, J. R. Parquette, Langmuir 2019, 35, 12460–12468.
- [20] H. Shao, T. Nguyen, N. C. Romano, D. A. Modarelli, J. R. Parquette, J. Am. Chem. Soc. 2009, 131, 16374 – 16376.
- [21] J. Gawroński, M. Brzostowska, K. Kacprzak, H. Kołbon, P. Skowronek, Chirality 2000, 12, 263 – 268.
- [22] H. Shao, J. Seifert, N. C. Romano, M. Gao, J. J. Helmus, C. P. Jaroniec, D. A. Modarelli, J. R. Parquette, *Angew. Chem. Int. Ed.* **2010**, *49*, 7688–7691; *Angew. Chem.* **2010**, *122*, 7854–7857.
- [23] H. C. Yang, R. Z. Waldman, M. B. Wu, J. Hou, L. Chen, S. B. Darling, Z. K. Xu, Adv. Funct. Mater. 2018, 28, 1705327.
- [24] a) B. P. Lee, J. L. Dalsin, P. B. Messersmith, *Biomacromolecules* 2002, 3, 1038–1047; b) Y. Wang, J. P. Park, S. H. Hong, H. Lee, *Adv. Mater.* 2016, 28, 9961–9968.
- [25] B. H. Kim, D. H. Lee, J. Y. Kim, D. O. Shin, H. Y. Jeong, S. Hong, J. M. Yun, C. M. Koo, H. Lee, S. O. Kim, Adv. Mater. 2011, 23, 5618 – 5622.
- [26] V. Ball, Colloids Surf. A 2010, 363, 92-97.
- [27] S. Bhattacharjee, J. Controlled Release 2016, 235, 337-351.
- [28] F. Tantakitti, J. Boekhoven, X. Wang, R. V. Kazantsev, T. Yu, J. Li, E. Zhuang, R. Zandi, J. H. Ortony, C. J. Newcomb, Nat. Mater. 2016, 15, 469.
- [29] W. Cheng, X. W. Zeng, H. Z. Chen, Z. M. Li, W. F. Zeng, L. Mei, Y. L. Zhao, ACS Nano 2019, 13, 8537 – 8565.

Manuscript received: January 23, 2020 Revised manuscript received: March 6, 2020 Accepted manuscript online: March 10, 2020 Version of record online: June 18, 2020